Combined experimental and numerical study on the near wake of a Darrieus VAWT under turbulent flows

Combined experimental and numerical study on the near wake of a Darrieus VAWT under turbulent flows

A Carbó Molina[1,3], T Massai[1], F Balduzzi[2], A Bianchini[2], G Ferrara[2], T De Troyer[3] and G Bartoli[1]

[1] Dept. of Civil and Environmental Engineering, Università degli Studi di Firenze, Via di Santa Marta 3, 50139, Firenze, Italy.
[2] Dept. of Industrial Engineering, Università degli Studi di Firenze, Via di Santa Marta 3, 50139, Firenze, Italy.
[3] Thermo and Fluid Dynamics (FLOW), Vrije Universiteit Brussel, Pleinlaan 2, 1050 Brussels, Belgium.

Corresponding author: andreu.carbo.molina@dicea.unifi.it

Abstract. Small Darrieus Vertical-Axis Wind Turbines (VAWTs) are presently seen as a relevant research topic for the wind energy community, since they are thought to perform better than horizontal-axis rotors in the complex and highly-turbulent flow typical of the urban environment. Indeed, a preliminary wind tunnel test campaign on a H-Darrieus VAWT showed a significant increase of the performance for high turbulence levels. The present study analyses in detail the near wake of the turbine in the same turbulent conditions, enabling a better insight on the reasons of this power increase, and on the means to take advantage of it. Near-wake measurements are also benchmarked with a CFD simulation of the entire wake, in order to match the experimental wake measurements with the detachment of flow structures observed in CFD simulations. By doing so, a deeper and useful insight on the reasons why VAWTs perform better in turbulent environments is gained.

Nomenclature

A_t	=	Turbine frontal area (m^2)
b	=	Grid bar width (m)
c	=	Turbine blade chord (m)
C_P	=	Power coefficient (-)
I_u	=	Intensity of turbulence in wind direction (-)
I_{per}	=	Periodic unsteadiness (-)
L_{ux}	=	Integral length scale of turbulence in wind direction (m)
M	=	Grid mesh size (m)
U	=	Wind speed (m/s)
R	=	Rotor radius (m)
P	=	Turbine mechanical power (W)
Re	=	Reynolds number (-)
x	=	Longitudinal distance from the rotor axis (m)
y	=	Transversal distance from the rotor axis (m)
$y+$	=	Dimensionless wall distance (-)
λ	=	Tip-speed ratio (-)

ω	=	Turbine rotational speed (rad/s)
Ω^*	=	Dimensionless Vorticity
CFD	=	Computational Fluid Dynamics
HAWTs	=	Horizontal-Axis Wind Turbines
rms	=	Root mean square
VAWTs	=	Vertical-Axis Wind Turbines
$_{sf}$	=	Optimal smooth flow conditions

1. Introduction

Even though the majority of studies in wind energy are presently being devoted at designing larger and larger rotors (e.g. [1]), there is also a significant interest arising on very small rotors for decentralized power production in the urban environment [2]. In doing so, however, new focus must be put on a better understanding of the physics of wind turbines under the complex inflow conditions (especially in terms of flow misalignment and turbulence levels) that are typical of similar installations [3]. Among other technologies, small Vertical-Axis Wind Turbines (VAWTs) are considered probably the most promising solution for the urban environment [4]. Despite their lower peak performance, some specific features like omnidirectionality, lower noise emissions and pleasant aesthetic appearance [5] have made them a valuable alternative to conventional Horizontal-Axis Wind Turbines (HAWTs) in urban applications [6-7]. Among the variety of VAWT designs, H-Darrieus turbines have especially attracted the attention of researchers, due to their higher efficiency and simple geometry [8].

The real suitability of wind turbines for use in the urban environment is, however, not straightforward. Most of the urban wind installations in fact fail to reach the expected energy yield [9, 10], resulting in still or underperforming turbines that also give bad press for the technology. The main issue that urban wind turbines face is that the wind conditions in the cities canopy layer are very complex. The wind typically has low intensity, high variability, high levels of turbulence, inclined and even reversed flows [11-13]. A careful analysis of these conditions is therefore mandatory for this technology to reach maturity and economic viability within an acceptable time horizon.

High turbulence is probably the most characteristic feature of urban flows. The study of its effect on VAWTs is up to now generally limited to on-field data by monitoring the performance of the installed turbines and the on-site wind turbulence measured by a meteorological station. Similar studies offer often unreliable and contradictory conclusions, as the effect of turbulence is said to be positive [14, 15], negative [16, 17] or velocity-dependent [18]. The impossibility to control all external conditions and influences in a real urban environment suggests that laboratory measurements might be necessary in order to obtain precise and repeatable turbine power rates and wake characteristics. However, replicating inside the wind tunnel the urban flow characteristics is not an easy task. In fact, most of the experimental facilities are designed for aeronautical purposes and have a very low background turbulence intensity (I_u < 1%). Conversely, the turbulence intensity inside the cities is often higher than 10% [13], and also the typical integral length scales of this turbulence are large compared with middle-sized wind tunnels, since values of L_{ux} in the order of 1 m may affect the turbine [19]. Several campaigns have analyzed VAWT performance inside the wind tunnel [20, 21], but only few of them addressed the topic of turbulence [22, 23], with not enough data available to support solid conclusions.

Starting from this background, an experimental set-up has been developed in the last few months at the Vrije Universiteit Brussel to evaluate the effect of turbulence on a H-Darrieus turbine performance in the wind tunnel [24]. A careful optimization of passive turbulence generating grids was carried out to allow setting the desired values of I_u and L_{ux} in the wind tunnel test section. The results showed a considerable boost in the performance of the turbine under highly turbulent flows [25].

The scope of the present study is to expand the knowledge on the effect of turbulence on a Darrieus VAWT, with special focus on the near wake of the turbine, which was recently shown to be of particular interest to understand the origin of flow macro-structures related with the blade-flow mutual interaction [26]. Regarding the effect of turbulence on the wake, a previous study [27] on a 5-bladed rotor detected large asymmetries and differences in the wake from smooth to turbulent flow. With the

same set-up as used in [24-25], a small two-bladed H-Darrieus rotor was exposed to different turbulence conditions, and the near-wake characteristics were measured in order to study the reasons of its performance increase. In addition, since direct spatially-resolved and comprehensive maps of the flow field (e.g. with particle image velocimetry) were not available, dedicated numerical simulations using computational fluid dynamics (CFD) were also carried out. This kind of simulations, if the proper levels of spatial and temporal refinement are provided [28], recently showed to be able to accurately reproduce the aerodynamics of Darrieus blades [29]. The computed flow fields allowed the identification of the main aerodynamic phenomena and flow macro-structures, whose traces were registered in the wake.

2. Methodology

2.1. Experimental tests

2.1.1. Facility

CRIACIV is an Inter-University Research Centre focused on the field of Building Aerodynamics and Wind Engineering, grouping eight Italian Universities. The Wind Engineering Laboratory is located in Prato, close to Florence, and it hosts an open-circuit boundary layer wind tunnel (Figure 1). The tunnel has a total length of about 22 m, including a nozzle at the inlet with a contraction ratio of 4.2 after the honeycomb and a T-diffuser at the outlet. The rectangular test section is 2.42 m wide and 1.60 m high. Air is aspired through a motor with a nominal power of 156 kW and the flow speed can be varied continuously up to ~ 30 m/s adjusting, by means of an inverter, the rotational speed of the fan and the pitch angle of its ten blades. In absence of turbulence generating devices, the free-stream turbulence intensity is around 0.7%.

2.1.2. Turbulence grids

To increase the level of free stream turbulence, squared-mesh wooden grids were placed in the boundary layer development zone of the wind tunnel (visible in Figure 1). Such grids are usually employed for studies on bluff bodies, but were here chosen for their simplicity and capability to provide a quasi-isotropic turbulence. Two grids were built to enable different combinations of I_u and L_{ux}. The design of the grids (described in Table 1) was done following the empirical relations found in literature [30-32], which describe the decay of turbulence downstream of the grid (Equations 1 and 2).

$$I_u = 2.58\left(\frac{x}{b}\right)^{-8/9} \tag{1}$$

$$L_{ux} = 0.2b\left(\frac{x}{b}\right)^{1/2} \tag{2}$$

Figure 1. View of the CRIACIV wind tunnel with turbulence grid 2 installed.

Table 1. Comparison of the turbulence grids used for the present tests.

Grid	Mesh size - M	Bar size - b	I_u range	L_{ux} range
1	10 cm	2.5 cm	2 – 5 %	5 – 7 cm
2	33 cm	7 cm	5 – 12 %	9 – 18 cm

2.1.3. Measurement system

The mean flow speed was monitored with a Pitot tube connected to a sensor Setra AccuSense model ASL. The free stream wind speed was set placing the Pitot tube in the test section, before the turbine was switched on. The spectral properties of the induced turbulence were determined through measurements with a Dantec single-component hot-wire probe 55P11 connected to a Dantec CTA 56C01 module and a 56C17 bridge. The spatial homogeneity of the flow at the position of the model was verified before the tests. The longitudinal integral length scale L_{ux} was calculated according to Taylor's frozen-eddy hypothesis as in [33], and the results were confirmed by fitting a von Kármán spectrum to the measured spectrum [34]. The turbulence intensity was calculated as usual by using the root mean square (*rms*) and the incoming longitudinal flow speed (Equation 3).

$$I_u = \frac{U_{rms}}{U_{free\_stream}} \tag{3}$$

Near wake measurements on the VAWT model tested within the CRIACIV wind tunnel test-section were performed by horizontally mounting a traversing system at a distance $x = 1.5R$ downstream the rotor, at its half height. Such test rig is composed by a stiff aluminium arm mounted on an endless-screw activated with a stepper motor controlled through an Arduino-based algorithm. Three probes were mounted on the rigid fork connected to the moving aluminum arm, one central Pitot tube, to measure the mean punctual flow speed, and two hot-wire probes for measuring the fluctuating component of longitudinal wind speed. In this way, an adequately refined wake profile has been obtained for each tested configuration. The test rig and the probes are visible in Figure 2.

2.1.4. Turbine model

The rotor is a two-blade H-type Darrieus turbine with two NACA0018 blades with a 5 cm chord (c) and two inclined struts per blade (Figure 2). Due to the small size of the rotor, angular speeds (and thus centrifugal loads) were high in order to achieve the suitable Reynolds numbers on the blades.

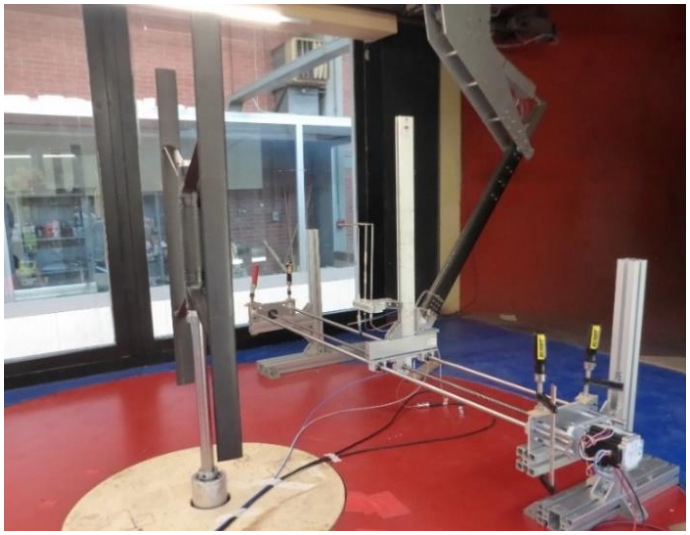

Figure 2. Turbine prototype and measurement rig with the probe behind it.

To ensure proper mechanical properties, the rotors were manufactured using carbon-epoxy composite. The VAWT rotor was connected via a torque sensor and a drive belt (with gear ratio 100/28) to a brushed-DC motor. This motor was used to drive the VAWT rotor during start-up, while it acted as a generator in normal operation. The electrical output of the motor was fed to a circuit of variable resistance for angular speed control. A torque sensor was used to measure the mechanical torque and angular speed (and thus mechanical power) of the VAWT. The torque sensor, drive belt, DC motor, and measurement equipment were housed inside an aluminium frame. The torque sensor was a Lorenz Messtechnik DR-3000 sensor with an accuracy of $\pm 2 \cdot 10^{-3}$ Nm. It was fitted between two torsionally-stiff couplings to allow for possible misalignments.

2.1.5. Experimental test conditions

Experiments were carried out in four different turbulence conditions to discriminate the effect of I_u and L_{ux} (Table 2). The incoming wind speed was set at U = 9 m/s during all tests, as it was the best operational point for the VAWT prototype, resulting in a mean chord-based Reynolds of around 10^5.

Table 2. Description of the different tests conditions in which the experiments were performed.

Condition	Grid	grid distance x	mean I_u	mean L_{ux}
Smooth flow	none	-	0.7 %	-
Low I_u	2	7.6 m	5.4 %	18 cm
High I_u	2	3.75 m	9.2 %	15 cm
Low I_u, low L_{ux}	1	2.1 m	4.6 %	4 cm

The turbine performance was monitored by measuring its power coefficient C_P (Equation 4) and tip-speed ratio λ (Equation 5). The near wake was characterized by the longitudinal wind speed deficit and the turbulence intensity I_u. Blockage may have an influence in the measurements and wake shape [35]; based on the solid blockage around only 10% and on the fact that all the measurements were taken with the same blockage conditions, no corrections were applied in this sense.

$$C_P = \frac{P}{\frac{1}{2}\rho A_t U^3} \tag{4}$$

$$\lambda = \frac{\omega R}{U} \tag{5}$$

2.2. Numerical analysis

Detailed unsteady Reynolds-Averaged Navier-Stokes (U-RANS) CFD simulations were carried out based on a consolidated numerical approach developed by some of the authors [36]. The 2D U-RANS approach might appear not entirely appropriate for this kind of analyses, since 2D models are deemed to predict vortices more coherent and less prone to breakdowns with respect to real 3D flow structures. Moreover, it could be argued that a RANS approach is not suitable to properly capture the effect of turbulence on the blade-flow interaction. This is indeed partially true, even if it should be remembered that the main scope of CFD simulations in the present work was to correlate the shape of the wake with the main aerodynamic phenomena taking place past rotating blades, while the study on the effect of turbulence was entirely assigned to experiments. Anyhow, the sound agreement found with respect to wind tunnel data in recent parallel studies [26, 29], and also during the present analysis, corroborated the suitability of this approach for a first - and computationally affordable - assessment of the wake characteristics and of the overall turbine performance.

In the simulations, carried out with the commercial software ANSYS® FLUENT®, the *k-ω SST* model was adopted for turbulence closure, according to the prescription of [36], and coupled with the Enhanced Wall Treatment embedded in the FLUENT® code for the computation of the boundary layer

in the near-wall regions. The coupled algorithm was chosen for pressure-velocity coupling, and the 2nd order upwind scheme was adopted for both RANS and turbulence equations. Inlet air conditions were the same as monitored during the experimental tests. The global convergence of each simulation was monitored by considering the difference between the mean values of the torque coefficient over two subsequent revolutions: according to [36], the periodicity error threshold was set to 0.1%. To simulate the rotation of the turbine, the sliding mesh technique was employed, i.e. the computed domain was split into a circular zone containing the turbine, rotating with the same angular velocity of the rotor, and an outer rectangular fixed zone, determining the overall domain extent. According to [28], the dimensions of the latter were not the ones of the wind tunnel, but they adopted the settings of [36], in order to avoid numerical blockage effects. The mesh was of unstructured and hybrid type, with triangular elements in the core flow region, and an O-grid made of quads in the boundary layer. The expansion ratio for the growth of elements starting from the surface was kept below 1.1 to achieve good mesh quality, ensuring a y^+ constantly < 1. The airfoil surface was discretized with 1400 nodes. The mesh characteristics (visual details are reported in Figure 3 and Figure 4) fully accomplished the criteria based on dimensionless thresholds proposed in [28]. Based on the same criteria, in order to limit the Courant Number in proximity of the blades, an angular timestep of 0.25° was used for the tip-speed ratios in the left-hand side of the curve, increasing to 0.40° in the right-hand side. With the described settings, the calculation time to achieve a complete revolution of the rotor is around 20 hours in a 16 CPUs (2.8 MHz each) calculation center. The required number of revolutions to achieve a periodic solution was variable between 15 and 25 revolutions.

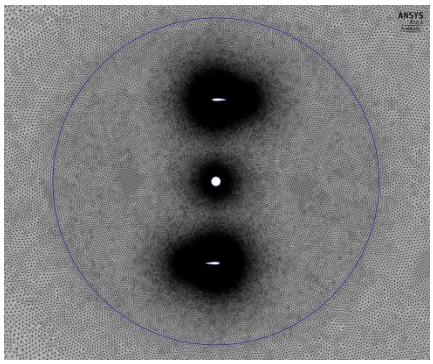

Figure 3. Visualization of the computational mesh of the turbine.

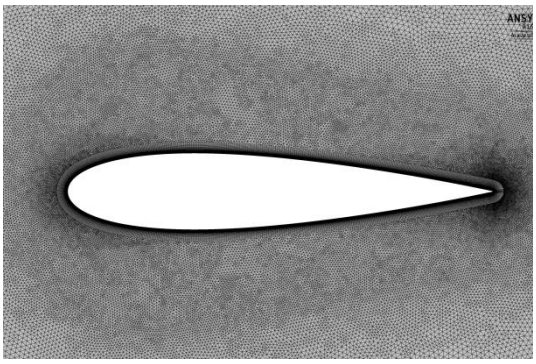

Figure 4. Detailed view of the mesh refinement near the airfoil.

3. Results

3.1. VAWT power curves under turbulent conditions

Figure 5 presents the power curves around the maximum efficiency obtained with the VAWT model in the turbulence conditions presented in Table 2. The results are also compared with the values coming from CFD simulations described in subsection 2.2. The values were normalized by the maximum C_P obtained under smooth flow conditions due to confidentiality reasons.

Upon examination of the experimental data, it is apparent that the increased I_u provided a notable increase of the turbine performance, up to +20% for the high turbulence case. On the other hand, the effect of L_{ux} was not so evident, as the two curves at $I_u \approx 5\%$ showed similar C_P values even when the L_{ux} levels were very different. It is worth noticing that the error bars are larger in the high turbulence case, because the wind speed profile is not completely uniform when the turbine is so close to the grid, and therefore the uncertainty in the wind speed is higher [24, 25]. As the computational cost of simulated C_P-λ points was very high, only 4 points of the curve were obtained, but it is apparent how the agreement with experimental data was considerably good. The following subsections will try to address the relation between this performance increase and the characteristics of the near wake.

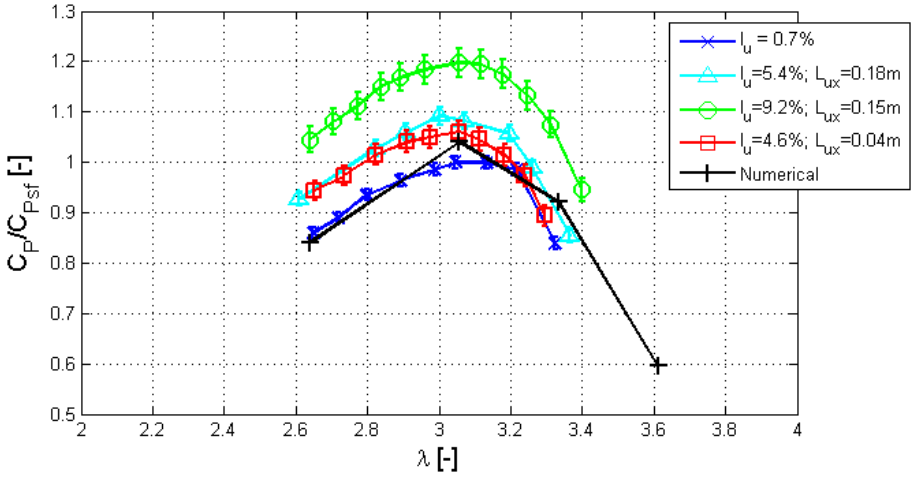

Figure 5. Power curves obtained with the VAWT under different turbulence conditions and in the numerical simulation, normalized with the optimum C_P in smooth flow.

3.2. Velocity deficit in the near wake of the VAWT

Figure 6 presents the axial wind speed profile at midplane downstream of the VAWT, taken at the optimal λ. The arrow shows the turbine sense of rotation. The effect of turbulence is not so evident in the wake shape; it seems to result only in a reduced speed deficit. Just behind the shaft, while the wind speed in smooth flow drops to the 20% of the free stream, in the high turbulence case the wind speed only drops to 30% of it. This would seem in conflict with the higher energy extraction made by the rotor, but can be easily explained if one considers that the turbulent flow is thought to promote a faster dissipation of the wake itself due to the more intense mixing with the surrounding wind stream. As in previous analyses, there is no evident effect of the free stream L_{ux}. The measurement uncertainty, considering random and propagation errors, is about 4% of the free stream windspeed.

In Figure 7 the experimental values are also compared to CFD simulation results. Good agreement is apparent both for the basic shape and for the acceleration of the flow around the turbine. However, the experimental wake is shifted to the right, maybe due to asymmetries of the incoming flow, and the maximum wind speed drop behind the shaft is underpredicted by the CFD simulation. Still, these results are in agreement with the findings of [29].

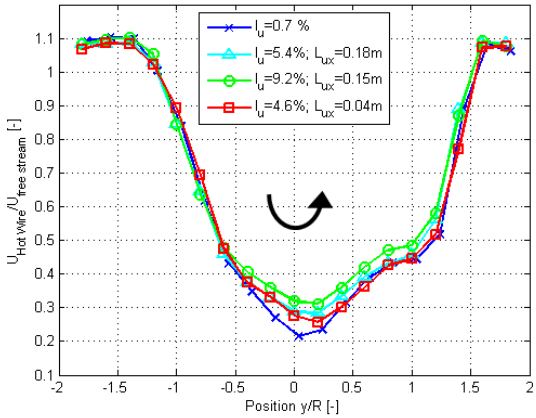

Figure 6. Normalized wind speed in the wake of the VAWT under different turbulence conditions.

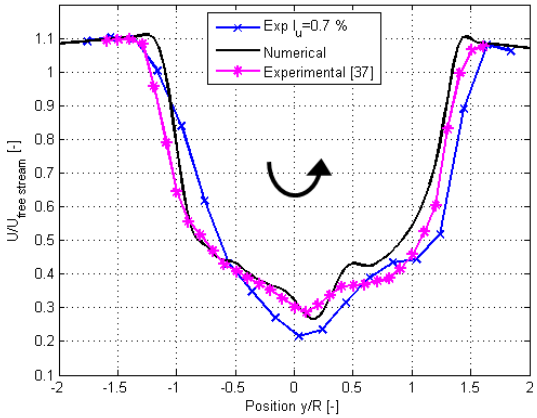

Figure 7. Comparison of the experimental and numerical wake wind speed, with experiments from Tescione et al. [37].

The wake shape was also compared with data from the most similar experiment found in literature. Tescione et al. [37] performed PIV measurements at 1.5*R* downstream of a 2-blade NACA0018 H-Darrieus at similar Reynolds numbers but higher λ (4.5 versus the present value of 3.05). This difference might explain the more pronounced wake shape for low λ, also observed in other studies [26]. The radial extension of the wake and the velocity levels downstream of the turbine are anyhow in fair agreement.

3.3. Turbulence intensity and periodic unsteadiness in the VAWT wake

Figure 8 describes the turbulence intensity measured in the wake for low, medium and high levels of turbulence, compared to numerical simulations. As one may notice, the shape of the turbulence distribution is correctly predicted by the numerical calculations, with one large peak at -*R*, a lower one at +1.4*R* (edges of the wake), and a third one representing the wake of the shaft. The reasons of these turbulence intensity peaks are readily noticeable by analyzing the computed flow field, reported in Figure 10 and Figure 11 in terms of axial wind speed and dimensionless vorticity Ω^* (defined in Equation 6), respectively.

$$\Omega^* = \frac{\frac{dU_y}{dx} - \frac{dU_x}{dy}}{U \cdot c} \tag{6}$$

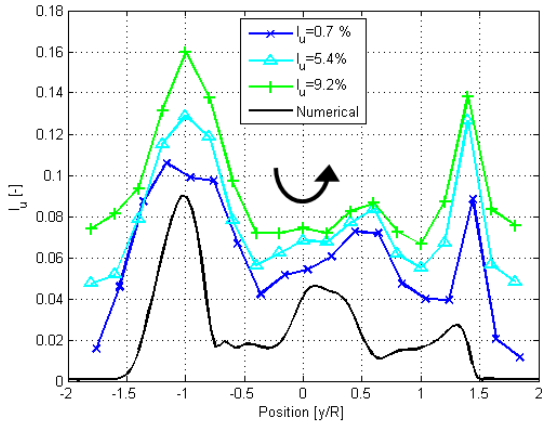

Figure 8. Turbulence intensity measured in the near wake, for three values of turbulence, compared with the numerical prediction.

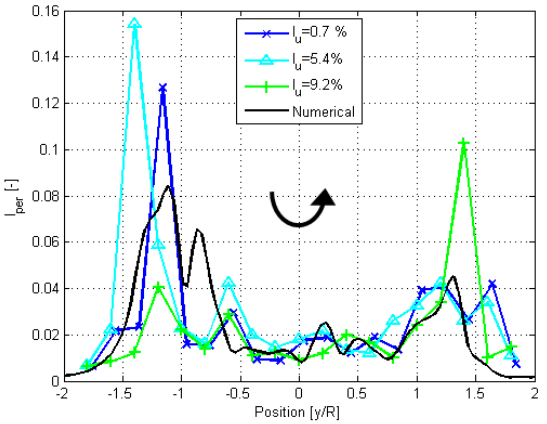

Figure 9. Wake periodic unsteadiness calculated from the experimental data at different I_u, compared with numerical simulations.

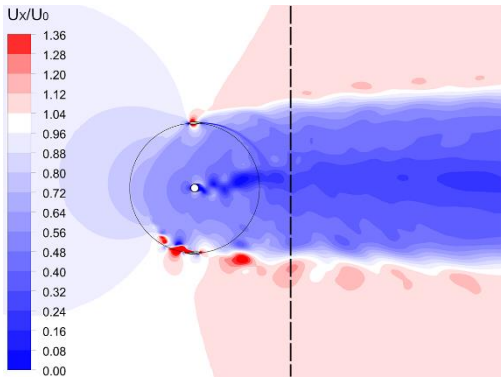

Figure 10. Instantaneous contour plots of dimensionless velocity, with the position of the traverse.

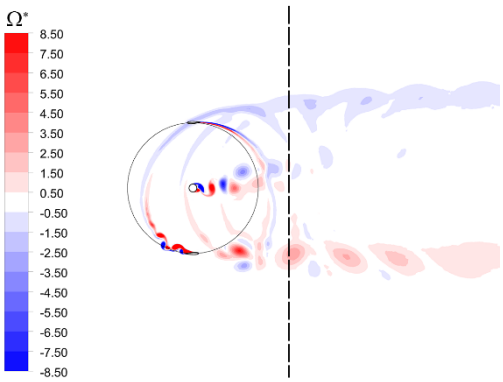

Figure 11. Instantaneous contour plots of dimensionless vorticity, with the position of the traverse.

Upon examination of the contour plots, it is apparent that the peaks in the turbulence intensity are related with the passage of high vorticity zones. These are in turn generated by: 1) the vortex shedding of the central tower (central peak); 2) the shed vorticity coming from the flow reattachment on the airfoil near the end of the downwind part of the revolution (peak at positive y/R); 3) the passage of the macro vortices that are detached from the airfoils as soon as they undergo deep stall conditions in the upwind region (higher peak at negative y/R). These latter ones are predominant and have a strong influence on the flow surrounding the blades in the first part of the downwind region. Based on these insights, it can be hypothesized that the main reason why macro-turbulence has a positive impact on the performance of a H-Darrieus VAWT is the improvement of the boundary layer stability on the airfoils, leading to a delayed onset of stall conditions (in terms of azimuthal position along the revolution) and then to different shed vorticity downstream. In particular, the increase of the turbulence intensity in the wake is less intense for the high-turbulence case in comparison to the mean turbulence levels, even if experiments clearly highlighted that, when increasing the free stream turbulence, the graph is basically shifted upwards (the free stream turbulence is not modelled numerically). Another remarkable feature that can be extracted from Figure 8 is that the wake of the shaft dims as I_u increases. In fact, for high turbulence the shaft is nearly "invisible", as the central peak is at the same level of the incoming free stream. This fact, which was predicted numerically in [38], can be another factor responsible for the increase of C_P. Measurement uncertainties for I_u values are of the order of $3 \cdot 10^{-3}$. To complete the analysis, the concept of periodic unsteadiness (I_{per}), originally described in [26], was used. The I_{per} tries to identify those flow structures that are mostly periodic during the revolution, i.e. directly correlated to specific positions of the blade. It is defined as the root mean square of the phase-resolved velocity, which is calculated as the ensemble average among values acquired at the same phase for all the different revolutions (purged by the time-mean value). Figure 9 shows the difficulty of phase-resolving experimental data where ω was not perfectly constant, but two regions of high periodic unsteadiness are clearly identifiable (for all levels of turbulence) between $1R$ and $1.5R$ at both sides of the wake. The numerical simulations show good agreement with the experimental data, and for high λ higher values appear towards the external boundaries of the wake [26], not due to vortices but to residual oscillations in the shear layer between the turbine wake and the undisturbed flow. The variability of I_{per} for increased levels of turbulence further corroborates the hypothesis that the oncoming turbulence strongly impacts on the location of stall on the airfoils, and then on the vortical structures that are detached from the airfoils and convected downstream.

4. Conclusions

The increasing number of installations in high-turbulence locations (as urban environments) urges the development of tailored experimental and CFD methods to optimize Darrieus VAWTs for complex inflows. In this study, turbulent grids allowed the authors to model nearly-urban wind conditions in the wind tunnel, with the additional possibility of isolating the effect of three flow parameters (U, I_u and L_{ux}). Experimental measurements showed that the turbulence intensity I_u has a large influence on the studied 2-blade turbine performance, increasing its power by 20% from smooth flow to I_u = 9.4 %. Conversely, integral length scales of this turbulence did not show to have relevant influence on the turbine power curves. The study of the near wake ($1.5R$ downstream the turbine) in turbulent conditions tried to find an explanation for this performance rise, and to increase the understanding of the inner flow physics. Wind speed measurements showed faster wake recovery for turbulent flows, as the wind speed drop was 10% lower than in smooth flow. The shape of the wake in that position did not show large differences from smooth to turbulent flows. Upon examination of the turbulence intensity profiles in the wake, it was also noticed that the effect of the shaft wake is minimized by the turbulence increase, probably reducing the detriment of the turbine performance related to it. Moreover, the results of dedicated unsteady CFD simulations highlighted that the peaks in the turbulence intensity are directly related with the alternate passage of high vorticity zones. These are in turn generated by: 1) the vortex shedding of the central tower (central peak); 2) the passage of

macro vortices that are detached from the airfoils as soon as they undergo deep stall conditions (higher peak at negative *y/R*); 3) the shed vorticity coming from the flow reattachment on the airfoils as soon as the incidence angle starts decreasing again in the downwind region (peak at positive *y/R*).
To conclude, the present study confirmed that VAWTs tend to perform better in turbulent flows, both for turbine production and wake recovery. These experiments, combined with the additional information coming from U-RANS CFD simulations, provide innovative and valuable data to understand their operation. Future work will be devoted to testing the rotor at other Reynolds numbers and tip-speed ratios in order to increase the knowledge on how the flow interacts with the blades; more wake distances will also studied in order to acquire useful information of practical use in designing VAWT array configurations for urban roofs.

Acknowledgements

The present research is part of the European Innovative Training Network (ITN) AEOLUS4FUTURE "Efficient Harvesting of the Wind Energy". The project is funded by the Horizon 2020 Research and Innovation program under the Marie Skłodowska-Curie grant agreement No. 643167. The support from Nenuphar is also gratefully acknowledged.

References

[1] Van Kuik GAM et al. 2016 Long-term research challenges in wind energy - a research agenda by the European Academy of Wind Energy, *Wind Energ. Sci.* **1** 1-39
[2] Mertens S 2006 *Wind Energy in the Built Environment* (Brentwood: Multi-Science)
[3] International Energy Agency (IEA) 2017 *IEA Wind TCP Annual Report - Task 27: Small Wind Turbines in High Turbulence Sites*
[4] Cooper P 2010 Development and analysis of vertical-axis wind turbines *Wind Power Generation and Wind Turbine Design*, ed. Wei Tong (Ashurst: WIT Press)
[5] Paraschivoiu I 2002 *Wind turbine design: with emphasis on Darrieus concept* (Monreal: Presses inter Polytechnique)
[6] Barlow JF and Drew DR 2015 Wind flow in the urban environment. WINERCOST Work-shop *Trends and Challenges for Wind Energy Harvesting*. Coimbra, Portugal.
[7] Balduzzi F et al. 2012 Feasibility analysis of a Darrieus vertical-axis wind turbine installation in the rooftop of a building *Appl Energy* **97** 921–929.
[8] Aslam Bhutta MM et al. 2012 Vertical axis wind turbine - A review of various configurations and design techniques *Renew Sust Energ Rev* **16** 1926-1939
[9] Bianchi S, Bianchini A, Ferrara G and Ferrari L 2014 Small wind turbines in the built environment: influence of flow inclination on the potential energy yield *J Turbomach* **136**
[10] Bianchini A, Ferrara G and Ferrari L 2015 Design guidelines for H-Darrieus wind turbines: Optimization of the annual energy yield, *En Conv Man* **89** 690-707
[11] Beller C 2009 *Urban Wind Energy - State of the Art 2009* Danmarks Tekniske Universitet, Risø Nationallaboratoriet for Bæredygtig Energi 1668(EN)
[12] Rabkin D and Tomusiak M 2012 *Museum of Science wind turbine lab report* (Boston)
[13] Janajreh I, Su L, Alan F 2013 Wind energy assessment: Masdar City case study *Ren Ene* **52** 8-15
[14] Möllerström E, Ottermo F, Goude A, Eriksson S, Hylander J and Bernhoff H 2016 Turbulence influence on wind energy extraction for a medium size vertical axis wind turbine *Wind Energ.* **19**
[15] Bertényi T, Wickins C and McIntosh S 2010 Enhanced energy capture through gust-tracking in the urban wind environment *48th AIAA Aerospace Sciences Meeting Including the New Horizons Forum and Aerospace Exposition* (Orlando, Florida, 2010)
[16] Pagnini LC, Burlando M, Repetto MP 2015 Experimental power curve of small-size wind turbines in turbulent urban environment *App Ene* **154**

[17] Kooiman SJ and Tullis SW 2010 Response of a vertical axis wind turbine to time varying wind conditions found within the urban environment *Wind Engineering* **34**(4)
[18] Lee KY, Tsao SH, Tzeng CW and Lin HJ 2018 Influence of the vertical wind and wind direction on the power output of a small vertical-axis wind turbine installed on the rooftop of a building *App Ene* **209**
[19] Dallman AR 2013 *Flow and turbulence in urban areas* PhD thesis - University of Notre Dame
[20] Sheldahl RE 1981 Comparison of field and wind tunnel Darrieus wind turbine data *Sandia National Laboratories energy report*.
[21] Dossena V, Persico G, Paradiso B, Battisti L, Dell'Anna S, Brighenti A and Benini E 2015 An experimental study of the aerodynamics and performance of a Vertical Axis Wind Turbine in a confined and unconfined environment *J Energy Resour Technol* **137**
[22] Miau JJ et al. 2012 Wind tunnel study on aerodynamic performance of small Vertical-Axis wind turbines (Cheng Kung University, Taiwan)
[23] Ahmadi-Baloutaki M, Carriveau R and Ting DSK 2015 Performance of a vertical axis wind turbine in grid generated turbulence *Sustainable Energy Technologies and Assessments* **11**
[24] Carbó Molina A, Bartoli G and De Troyer T 2017 Wind tunnel testing of small Vertical-Axis Wind Turbines in turbulent flows X *International Conference on Structural Dynamics, EURODYN* (Rome, Italy)
[25] Carbó Molina A, Bartoli G and De Troyer T 2017 2018 Generation of uniform turbulence profiles in the wind tunnel for urban VAWT testing *Wind Energy Exploitation in Urban Environment. TUrbWind 2017 Colloquium* (Springer)
[26] Bianchini A, Balduzzi F, Ferrara G, Ferrari L, Persico G, Dossena V and Battisti L 2017 Detailed analysis of the wake structure of a straight-blade H-Darrieus wind turbine by means of wind tunnel experiments and CFD simulations *J. Eng. Gas Turbines Power* **140**(3)
[27] Peng HY and Lam HF 2016 Turbulence effects on the wake characteristics and aerodynamic performance of a straight-bladed vertical axis wind turbine by wind tunnel tests and large eddy simulations *Energy* **109**
[28] Balduzzi F, Bianchini A, Ferrara G and Ferrari L 2016 Dimensionless numbers for the assessment of mesh and timestep requirements in CFD simulations of Darrieus wind turbines *Energy* **97**(15 Feb 2016) 246-261
[29] Bianchini A, Balduzzi F, Bachant P, Ferrara G and Ferrari L 2017 Effectiveness of two-dimensional CFD simulations for Darrieus VAWTs: a combined numerical and experimental assessment *En Conv Man* **136**(15 March 2017) 318-328
[30] Laneville A 1973 Effects of turbulence on wind induced vibrations of bluff cylinders Ph.D. thesis, University of British Columbia (Vancouver, Canada)
[31] Roach PE 1982 The generation of nearly isotropic turbulence by means of grids *Int. J. of Heat and Fluid Flow* **8**(2)
[32] Bearman PW and Morel T 1982 Effect of free stream turbulence on the flow around bluff bodies *Progress in Aerospace Sciences* **20**(2)
[33] Mannini C, Marra AM, Pigolotti L and Bartoli G 2015 Unsteady pressure and wake characteristics of a benchmark rectangular section in smooth and turbulent flow *14th International Conference on Wind Engineering*, Porto Alegre, Brazil
[34] Burton T 2001 *Wind Energy Handbook* (london: John Wiley & Sons)
[35] Li Q, et al. 2016 Study on power performance for straight-bladed vertical axis wind turbine by field and wind tunnel test *Ren Ene* **90**
[36] Balduzzi F, Bianchini A, Maleci R, Ferrara G and Ferrari L 2016 Critical issues in the CFD simulation of Darrieus wind turbines *Ren Ene* **85**(01) 419-435
[37] Tescione G, Ragni D, He C, Simão Ferreira CJ, van Bussel GJW 2014 Near wake flow analysis of a vertical axis wind turbine by stereoscopic particle image velocimetry. *Ren Ene* **70** 47-61
[38] Rezaeiha A, Kalkman I, Montazeri H, Blocken B 2017 Effect of the shaft on the aerodynamic performance of urban vertical axis wind turbines *En Conv Man* **149** 616–630